REFERENCES

Bonzon C, Bouchier-Hayes L, Pagliari LJ, Green DR, Newmeyer DD (2006). Caspase-2-induced apoptosis requires bid cleavage: a physiological role for bid in heat shock-induced death. *Mol Biol Cell* **17**: 2150-2157.

Chawla-Sarkar M, Leaman DW, Borden EC (2001). Preferential induction of apoptosis by interferon (IFN)-beta compared with IFN-alpha2: correlation with TRAIL/Apo2L induction in melanoma cell lines. *Clin Cancer Res* **7**: 1821-1831.

Chawla-Sarkar M, Leaman DW, Jacobs BS, Borden EC (2002). IFN-beta pretreatment sensitizes human melanoma cells to TRAIL/Apo2 ligand-induced apoptosis. *J Immunol* **169**: 847-855.

Chawla-Sarkar M, Lindner DJ, Liu YF, Williams BR, Sen GC, Silverman RH, Borden EC (2003). Apoptosis and interferons: role of interferon-stimulated genes as mediators of apoptosis. *Apoptosis* **8**: 237-249.

Chen Q, Gong B, Mahmoud-Ahmed AS, Zhou A, Hsi ED, Hussein M, Almasan A (2001). Apo2L/TRAIL and Bcl-2-related proteins regulate type I interferon-induced apoptosis in multiple myeloma. *Blood* **98**: 2183-2192.

Fisher PB, Prignoli DR, Hermo H, Weinstein IB, Pestka S (1985). Effects of combined treatment with interferon and mezerein on melanogenesis and growth in human melanoma cells. *J Interferon Res* **5**: 11-22.

Griffith TS, Chin WA, Jackson GC, Lynch DH, Kubin MZ (1998). Intracellular regulation of TRAIL-induced apoptosis in human melanoma cells. *J Immunol* **161**: 2833-2840.

Kang DC, Gopalkrishnan RV, Lin L, Randolph A, Valerie K, Pestka S, Fisher PB (2004). Expression analysis and genomic characterization of human melanoma differentiation associated gene-5, mda-5: a novel type I interferon-responsive apoptosis-inducing gene. *Oncogene* **23**: 1789-1800.

Kimberley FC, Screaton GR (2004). Following a TRAIL: update on a ligand and its five receptors. *Cell Res* **14**: 359-372.

Kubota T, Yokosawa N, Yokota S, Fujii N (2001). C terminal CYS-RICH region of mumps virus structural V protein correlates with block of interferon alpha and gamma signal transduction pathway through decrease of STAT 1-alpha. *Biochem Biophys Res Commun* **283**: 255-259.

Leaman DW, Chawla-Sarkar M, Jacobs B, Vyas K, Sun Y, Ozdemir A, *et al* (2003). Novel growth and death related interferon-stimulated genes (ISGs) in melanoma: greater potency of IFN-beta compared with IFN-alpha2. *J Interferon Cytokine Res* **23**: 745-756.

Meng RD, El-Deiry WS (2001). p53-independent upregulation of KILLER/DR5 TRAIL receptor expression by glucocorticoids and interferon-gamma. *Exp Cell Res* **262**: 154-169.

Merchant MS, Yang X, Melchionda F, Romero M, Klein R, Thiele CJ, *et al* (2004). Interferon gamma enhances the effectiveness of tumor necrosis factor-related apoptosis-inducing ligand receptor agonists in a xenograft model of Ewing's sarcoma. *Cancer Res* **64**: 8349-8356.

Morrison BH, Tang Z, Jacobs BS, Bauer JA, Lindner DJ (2005). Apo2L/TRAIL induction and nuclear translocation of inositol hexakisphosphate kinase 2 during IFN-beta-induced apoptosis in ovarian carcinoma. *Biochem J* **385**: 595-603.

Pfeffer LM, Dinarello CA, Herberman RB, Williams BR, Borden EC, Bordens R, *et al* (1998). Biological properties of recombinant alpha-interferons: 40th anniversary of the discovery of interferons. *Cancer Res* **58**: 2489-2499.

Ren DH, Mayhew E, Hay C, Li H, Alizadeh H, Niederkorn JY (2004). Uveal melanoma expression of tumor necrosis factor-related apoptosis-inducing ligand (TRAIL) receptors and susceptibility to TRAIL-induced apoptosis. *Invest Ophthalmol Vis Sci* **45**: 1162-1168.
Samraj AK, Sohn D, Schulze-Osthoff K, Schmitz I (2007). Loss of caspase-9 reveals its essential role for caspase-2 activation and mitochondrial membrane depolarization. *Mol Biol Cell* **18**: 84-93.
Shin S, Lee Y, Kim W, Ko H, Choi H, Kim K (2005). Caspase-2 primes cancer cells for TRAIL-mediated apoptosis by processing procaspase-8. *EMBO J* **24**: 3532-3542.
Stark GR, Kerr IM, Williams BR, Silverman RH, Schreiber RD (1998). How cells respond to interferons. *Annu Rev Biochem* **67**: 227-264.
van Loo G, Saelens X, Matthijssens F, Schotte P, Beyaert R, Declercq W, Vandenabeele P (2002). Caspases are not localized in mitochondria during life or death. *Cell Death Differ* **9**: 1207-1211.
Vogler M, Dürr K, Jovanovic M, Debatin KM, Fulda S (2007). Regulation of TRAIL-induced apoptosis by XIAP in pancreatic carcinoma cells. *Oncogene* **26**: 248-257.
Wagner KW, Engels IH, Deveraux QL (2004). Caspase-2 can function upstream of bid cleavage in the TRAIL apoptosis pathway. *J Biol Chem* **279**: 35047-35052.
Zhang L, Fang B (2005). Mechanisms of resistance to TRAIL-induced apoptosis in cancer. *Cancer Gene Ther* **12**: 228-237.
Zhivotovsky B, Orrenius S (2005). Caspase-2 function in response to DNA damage. *Biochem Biophys Res Commun* **331**: 859-867.
Zhivotovsky B, Samali A, Gahm A, Orrenius S (1999). Caspases: their intracellular localization and translocation during apoptosis. *Cell Death Differ* **6**: 644-651.

**Figure legends**

Figure 1. Cell growth curve after treatment with intereferon (IFN)- $\alpha$ 2 and IFN- $\beta$. Each cell line was plated in 96 well plate with $1\times10^3$ cells/well. The cell numbers of four cell lines after treatment with 1000 IU/ml of IFN-□2 and IFN-□ for 24, 48, 72 h were measured by gentian violet dye-binding assay. Values are the means of three separate experiments with SD <10%. The absorbance of each cell line was measured at 595 nm by microplate reader. (△): non-treated, (▪): IFN- $\alpha$ 2, (×): IFN- $\beta$.

Figure 2. Cell viability after treatment with IFN- $\alpha$ 2 and IFN- $\beta$.
Each cell lines were plated in 96 well plate with $1\times10^3$ cells/well. The cell lines were treated with the presence of 1000 IU/ml of IFN- $\alpha$ 2 and IFN- $\beta$ for 72 h. Cell viability of treated cell was determined by the formazan-formation assay at 72 h in triplicate. The results are expressed as relative values (mean±S.D.) to non treated control. Non-treated: empty box, IFN- $\beta$ : slash mark box, IFN- $\beta$ : dotted box. *, significant ($P$<0.01) difference from the value in the untreated controls.

Figure 3. mRNA expression of IFN stimulated genes after treatment with IFN- $\alpha$ 2 and IFN- $\beta$.
The cell lines were plated in 24 well plate with $3\times10^3$ cells/well. After the presence of 1000 IU/ml of IFN- $\alpha$ 2 and IFN- $\beta$ for 24 h, total RNA was extracted. cDNA was synthesized from total extracted RNA (50 ng). The quantitative of the PCR was validated by the linearity of the determination of curve at various concentration of

cDNA. *MDA-5*; melanoma differentiation associated gene-5, *PKR*; double-stranded RNA-activated protein kinase, *MXA*; Myxovirus resistance protein A, *TRAIL*; tumor necrosis factor related apoptosis-inducing ligand, N; untreated group, α; treatment with IFN-α, β; treatment with IFN-β

Figure 4. FACS analysis of sub-$G_0$ populations.
Cells were plated on 10 cm dish plate with $2\times10^4$ cell/well. The cell lines were treated with the presence of 1000 IU/ml of IFN-β. After 72 h, cells were fixed with 70% ethanol for overnight at -20℃ and sub-$G_0$ populations were analyzed by FACS as described in Materials and Method. M1; sub-$G_0$ population.

Figure 5. FACS analysis of DNA fragmentation by TUNEL assay.
Cells were plated on 10 cm dish plate with $2\times10^4$ cell/well. The cell lines were treated with the presence of 1000 IU/ml of IFN-β. After 72 hours, cells were harvested and fixed. Cells were labeled with bromo-dUTP (BrdU) by the enzyme TdT, and then stained with FITC-labeled anti-BrdU antibody. The percentage of FITC-positive cells was assessed by FACS.

Figure 6. Caspase assay after treatment with IFN-β.
Cells were plated on 10 cm dish plate with $2\times10^4$ cell/well ($2\times10^5$ cell/well). The cell lines were treated with the presence of 1000 IU/ml of IFN-β in triplicate. After 72 hours, cells were harvested and caspase activity was assessed by caspase fluorometric assay as manufacturer's protocol. The caspase activity is expressed as the fold increase compared with the untreated cells. The results are expressed as relative values (mean±S.D.) to non treated control. Non-treated: empty box, IFN-β: dotted box. *; significant ($P<0.01$) difference from the value in the untreated controls.

Fig 7. IFN-β pretreatment sensitizes melanoma cell line against TRAIL mediated apoptosis
(a) G361, IFN-resistant cell, was plated in 96 well plate with $1\times10^3$ cells/well. Cells were treated with TNF-β, anti-Fas (CD95) antibody, TRAIL for 48 h at the concentration of 50 ng/ml, 500 ng/ml, 100 ng/ml respectively, or with 1000 IU/ml of IFN-β (24h) pretreatment followed by apoptosis inducing ligands for 48 h at the same concentration as above. Cell viability of treated cell was determined by the formazan-formation assay in triplicate. The results are expressed as relative values (mean±S.D.) to non treated control. (b) G361 was plated in 10 cm dish with $2\times10^4$ cells/well. Cells were treated with TRAIL for 24 h at the concentration of 100 ng/ml, or with 1000 IU/ml of IFN-β (24h) pretreatment followed with PBS wash and addition of TRAIL for 24 h at the same concentration as above. Cells were harvested and caspase activity was assessed by caspase fluorometric assay as manufacturer's protocol. The caspase activity is expressed as the fold increase compared with the untreated cells. TRAIL; tumor necrosis factor related apoptosis-inducing ligand, TNF-□; tumor necrosis factor-alpha, *; significant ($P<0.01$) difference.

Figure 1.

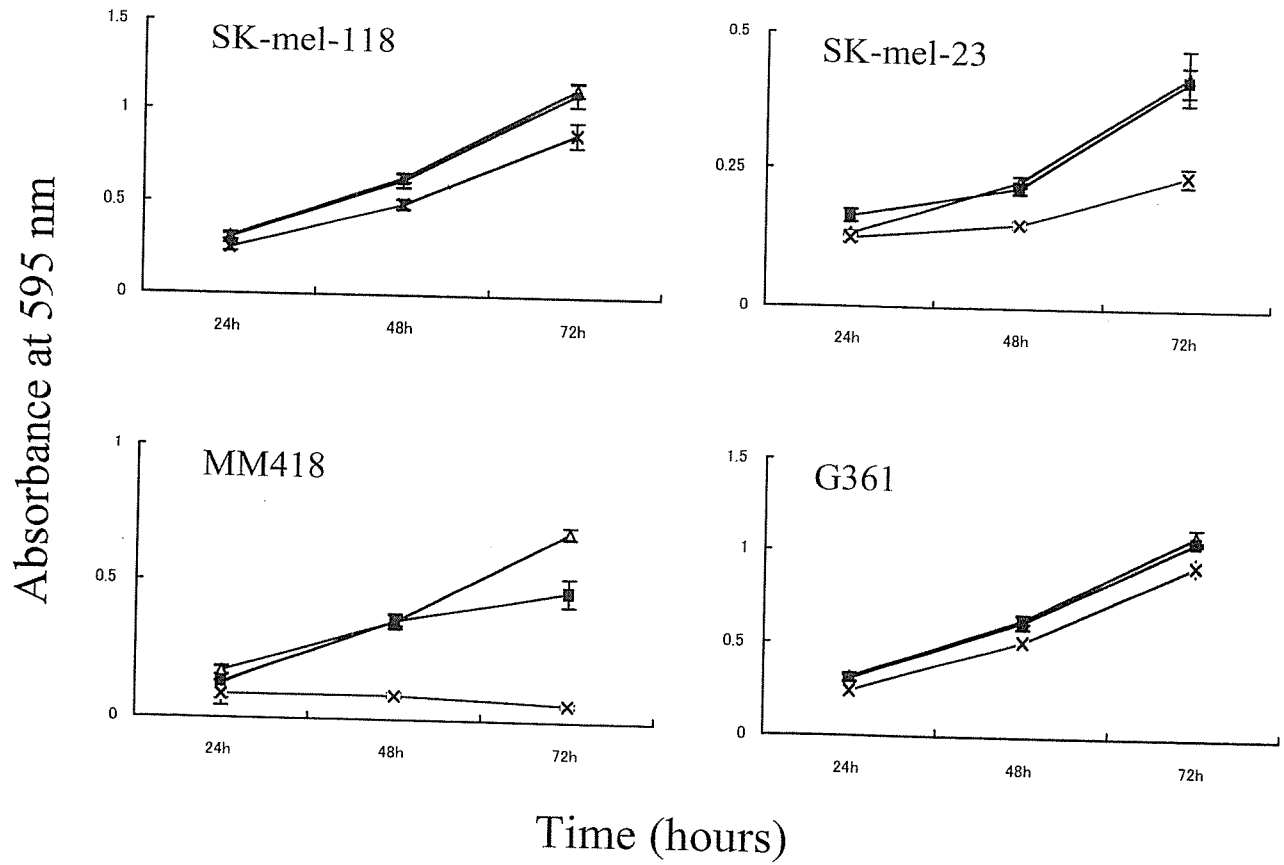
SK-mel-118
SK-mel-23
MM418
G361
Absorbance at 595 nm
Time (hours)
24h
48h
72h

Figure 2.

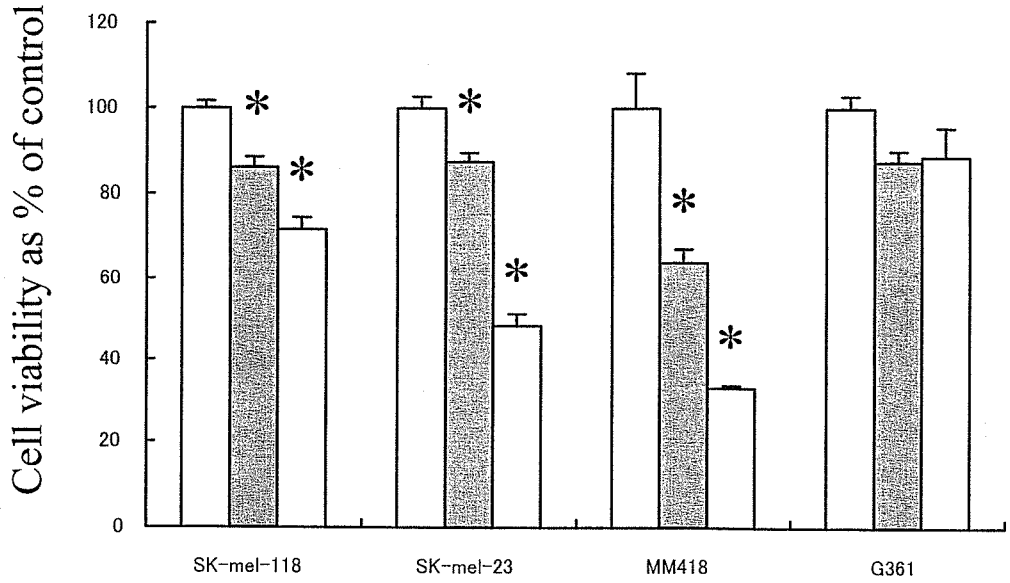
Cell viability as % of control
120
100
80
60
40
20
0
*
*
*
*
*
*
SK-mel-118
SK-mel-23
MM418
G361

Figure 3.

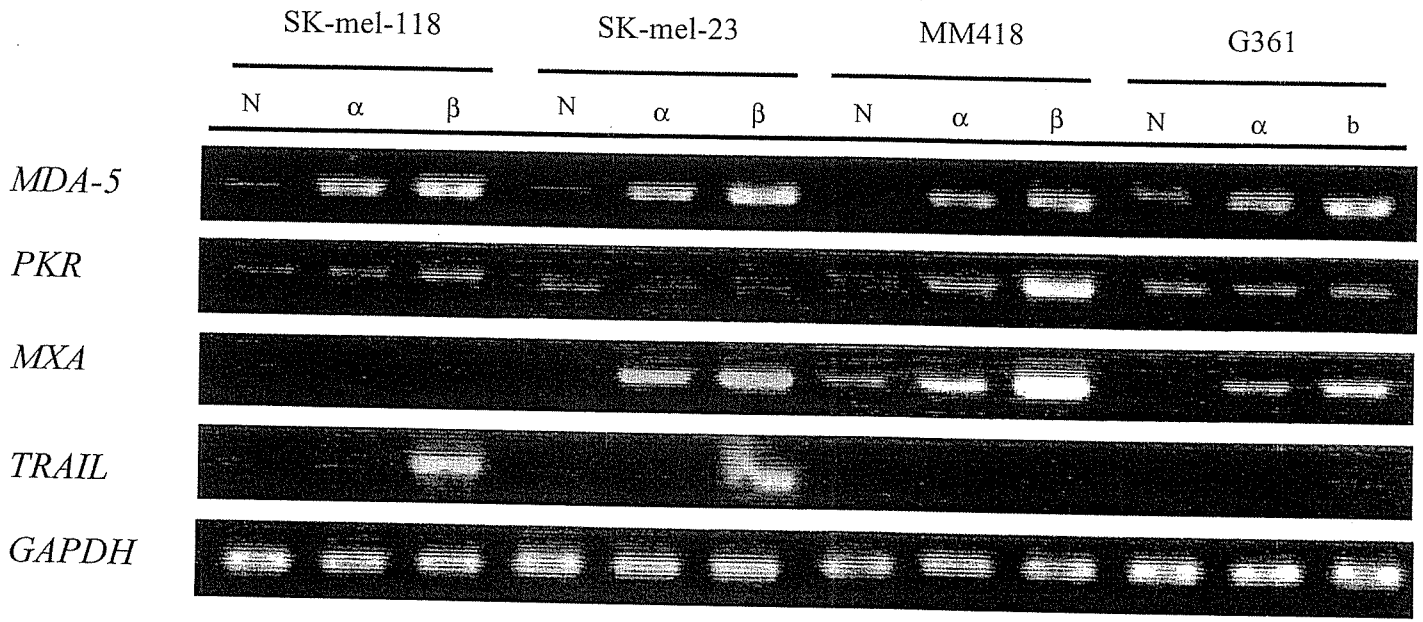
SK-mel-118
SK-mel-23
MM418
G361
N
α
β
N
α
β
N
α
β
N
α
b
MDA-5
PKR
MXA
TRAIL
GAPDH

Figure 4.

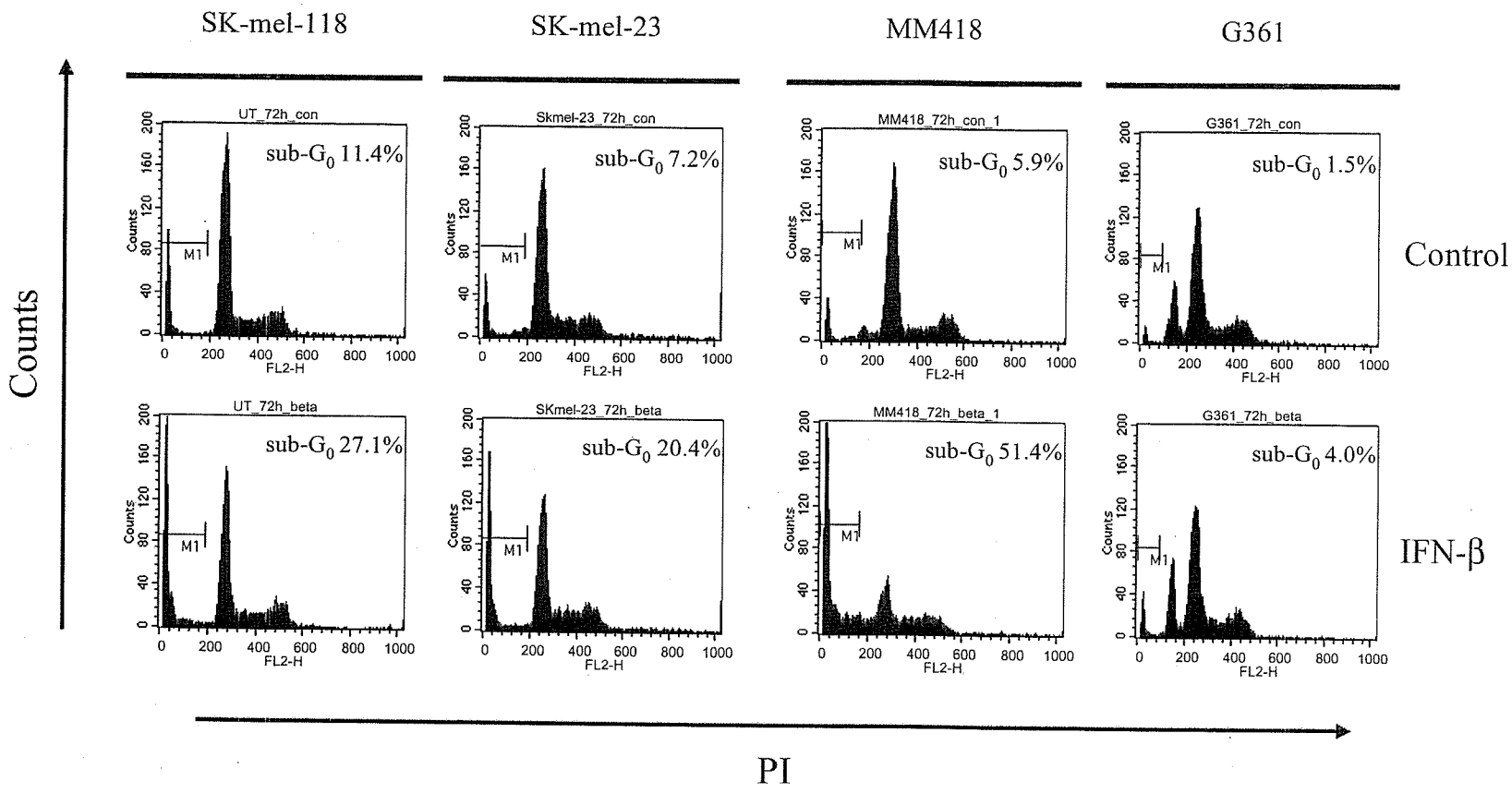
SK-mel-118
SK-mel-23
MM418
G361
Counts
PI
Control
IFN-β
UT_72h_con
sub-G0 11.4%
Skmel-23_72h_con
sub-G0 7.2%
MM418_72h_con_1
sub-G0 5.9%
G361_72h_con
sub-G0 1.5%
UT_72h_beta
sub-G0 27.1%
SKmel-23_72h_beta
sub-G0 20.4%
MM418_72h_beta_1
sub-G0 51.4%
G361_72h_beta
sub-G0 4.0%
M1
FL2-H

Figure 5.

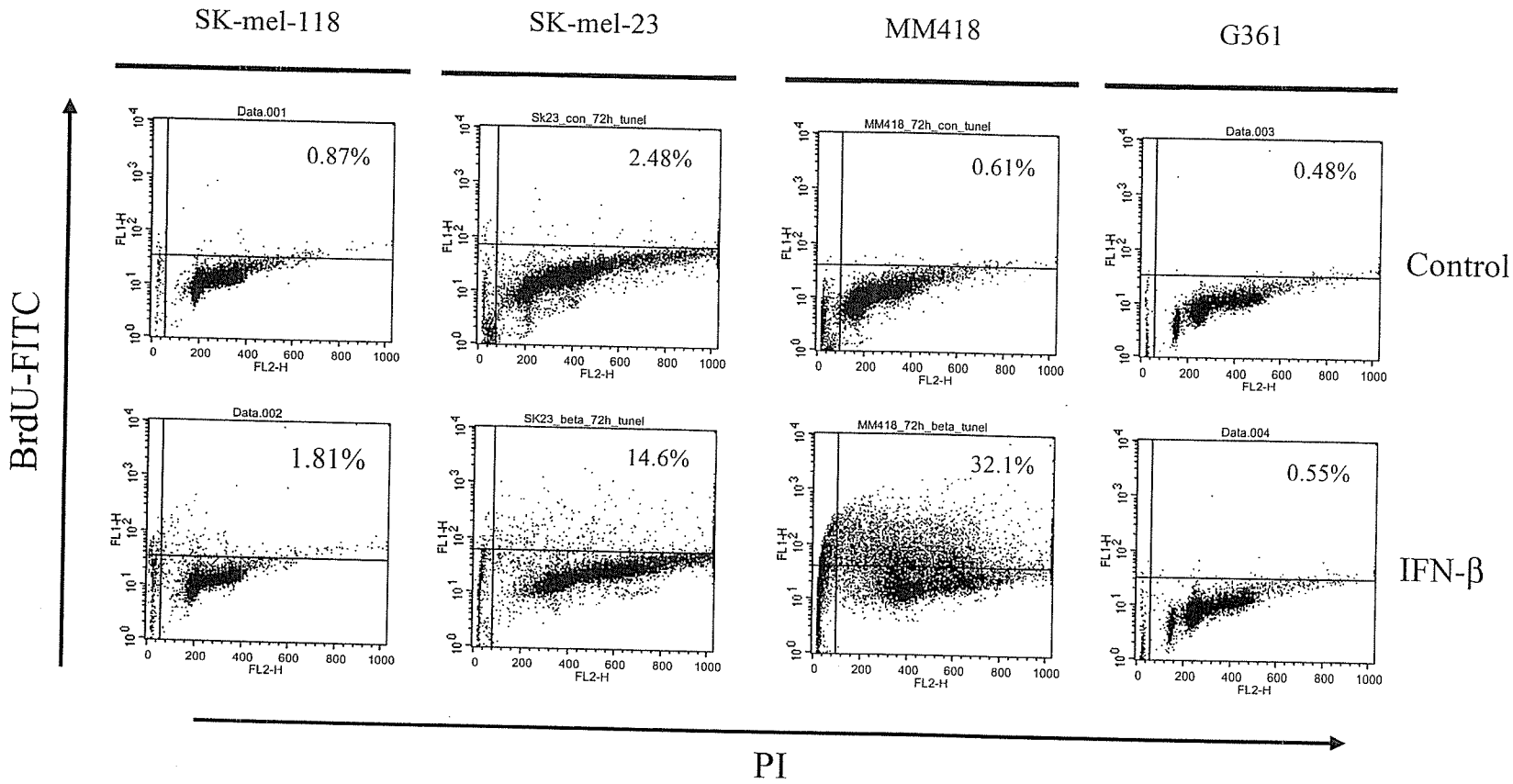
SK-mel-118
SK-mel-23
MM418
G361
Data.001
0.87%
Sk23_con_72h_tunel
2.48%
MM418_72h_con_tunel
0.61%
Data.003
0.48%
Control
Data.002
1.81%
SK23_beta_72h_tunel
14.6%
MM418_72h_beta_tunel
32.1%
Data.004
0.55%
IFN-β
BrdU-FITC
PI
FL1-H
FL2-H

Figure 6.

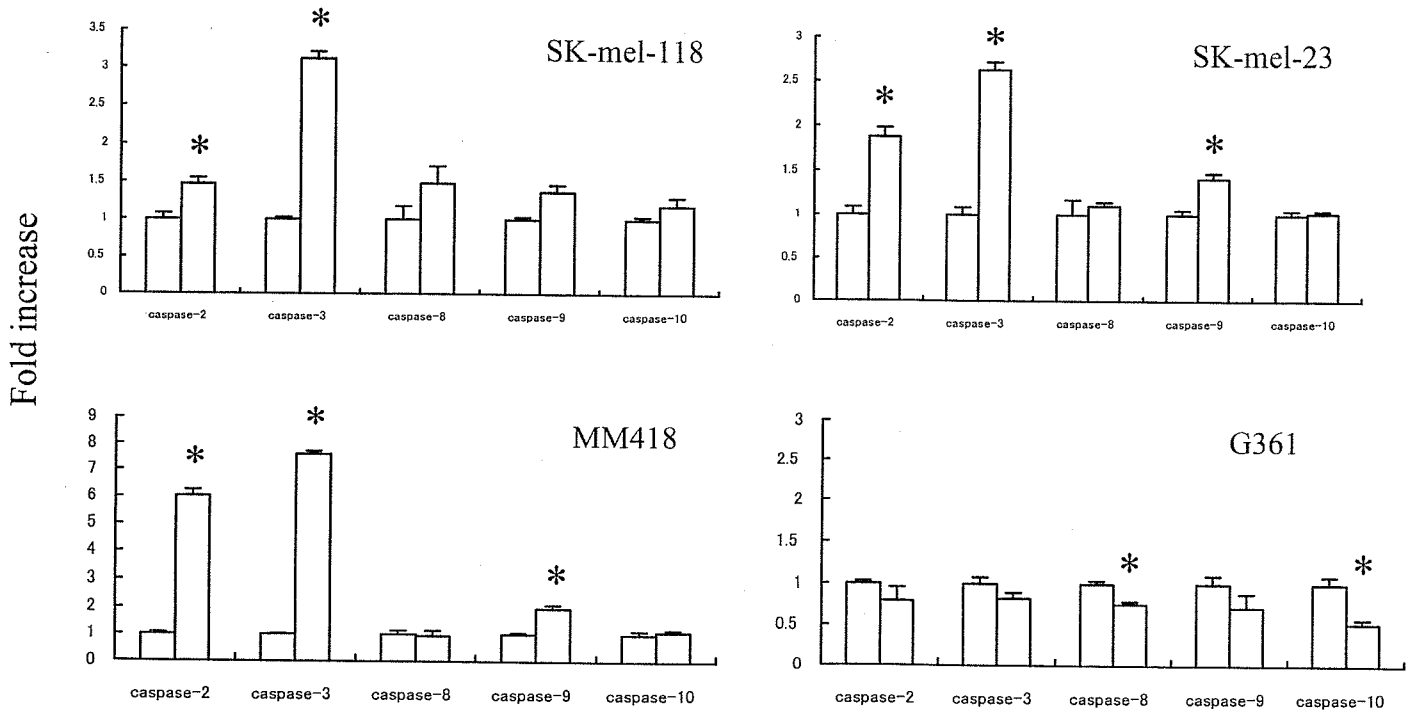
Fold increase
SK-mel-118
SK-mel-23
MM418
G361
caspase-2
caspase-3
caspase-8
caspase-9
caspase-10

Figure 7.

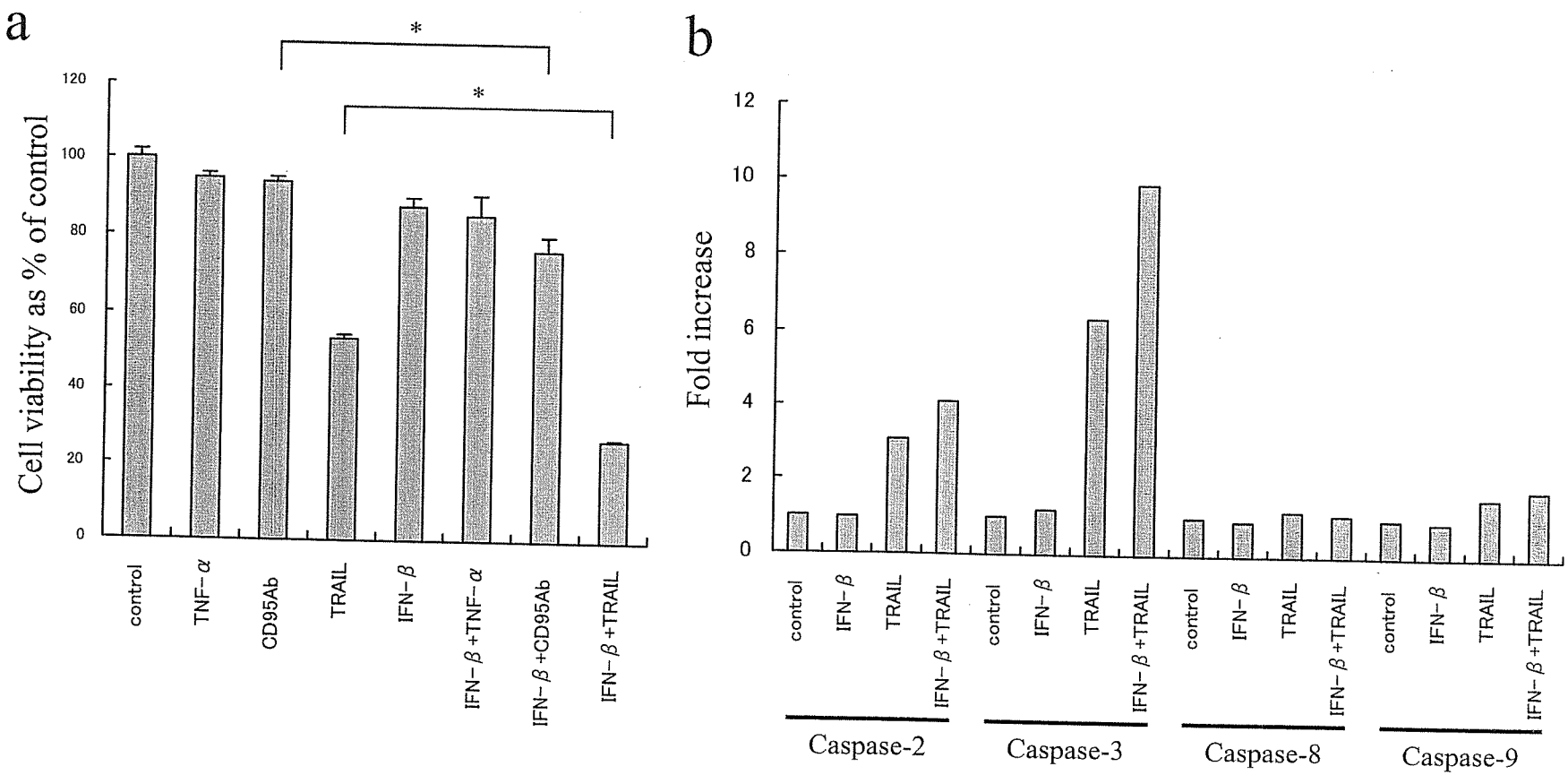
a
Cell viability as % of control
120
100
80
60
40
20
0
*
*
control
TNF-α
CD95Ab
TRAIL
IFN-β
IFN-β +TNF-α
IFN-β +CD95Ab
IFN-β +TRAIL
b
Fold increase
12
10
8
6
4
2
0
control
IFN-β
TRAIL
IFN-β +TRAIL
Caspase-2
Caspase-3
Caspase-8
Caspase-9

# Pilot study of combined dermoscopy and reflectance confocal microscopy evaluation for the early detection of basal cell carcinoma

Jiro Ogino, MD, Toshiharu Yamashita, MD, PhD, Ichiro Ono, MD, PhD, Akiko Sakemoto, MD, Takafumi Kamiya, MD, Rie Kaneko, MD, Kuninori Hirosaki, MD, PhD, Kenji Saga, MD, PhD, and Kowichi Jimbow, MD, PhD, FRCPC
Department of Dermatology, Sapporo Medical University School of Medicine, Sapporo, Japan

Correspondence and reprint requests:
Kowichi Jimbow MD, PhD, FRCPC
Department of Dermatology, Sapporo Medical University School of Medicine
Chuo-ku, Minami 1, Nishi 16, Sapporo, Japan
Phone: 81-11-611-2111 Fax: 81-11-613-3739 E-mail: jimbow@sapmed.ac.jp

References: 16, tables: 1, figures: 3
Running head: RCM detection of early/micro BCC
This study was supported in part by Grants-in-Aid from the Ministry of Education, Sports and Culture of Japan, and Ministry of Health, Labour and Welfare of Health and Labour Sciences Research Grants of Research on Advanced Medical Technology. A part of this study is also supported by Stiefel Inc.

**Summary**
**Background:** Dermosocopy has improved the diagnostic accuracy of pigmented melanocytic tumors (melanoma and pigmented nevi). It has, however, still limitation to diagnose pigmented non-melanocytic ones such as "early/ micro" basal cell carcinomas (BCCs).. Reflectance confocal microscopy (RCM) may be an additional tool because it can visualize living tumor tissues or cells at the level of histological resolution, and produces images representing horizontal planes of the skin. RCM can also provide three-dimensional reconstruction of tumors by stored-serial confocal images.
**Objectives:** This study investigates if the diagnosis of pigmented BCCs, specically their "early/micro" lesions can be improved by combined observation of dermoscopy and RCM.
**Methods:**
Five BCC lesions from four patients were investigated by dermoscopy and subsequently by *in vivo* or *ex vivo* RCM, i.e., RCM examination before and after surgical excision respectively. Dermoscopic observation followed the two-step method of the "consensus net meeting on dermoscopy 2000".
**Results:** In "early" BCC lesions, dermoscopy visualizes variegated pigmentation, multiple blue-gray dots or globules and spoke-wheal areas. RCM could easily visualize spoke-wheel like structures, dark areas and globular tumor-surface structures.. RCM could also identify their inside sub-structure, i.e., "dark area" surrounding the tumor-cell nests, which is a valuable diagnostic sign for "early" lesions of BCC.
**Conclusions:** RCM can be an additional tool for dermoscopy in identifying "early" lesions of pigmented BCC. The"dark area" surrounding tumor island is an important sign unique to these "early" lesions.
**Key words:** basal cell carcinoma, dermoscopy, reflectance confocal microscopy...

The incidence of skin cancers, melanoma and non-melanoma is rising. Its related serious consequences from improper management are an emerging healthcare problem, stressing the need for better diagnostic screening approaches as well as accurate tumor invasion evaluation. To minimize invasive procedures through the effective application of non-invasive imaging technologies is an important potential development in the tumor

invasion evaluation. These non-invasive technologies include dermoscopy, ultrasound, topography、tomogaraphy and reflectance confocal microscopy (RCM) .

Dermoscopy has been most extensively and commonly used recently for diagnosis of skin tumors,[1] but may have a limited value in evaluating tumor invasion. High-resolution ultrasound reflex transmission imaging and digital photography were compared between melanoma and nevi in order to better diagnose the pigmented skin tumors. However, accurate registration of the reflex transmission imaging with a corresponding photograph was crucial and only possible when corresponding points could be reliably identified on both images..[2] Relief patterns of the surface of benign and malignant skin tumors including basal cell carcinomas (BCCs) were analyzed by microtopography. Microtopographic inspection of skin tumor surface showed a significant decrease in the skin surface of BCCs compared to healthy skin surface, but this decrease was not high enough compared to that of melanocytic nevi. The *in vivo* optical coherence tomography was also carried out for BCCs but was found to be insufficient for identifying their subtypes.[3] RCM has been introduced recently in clinical dermatology,[4-11] including *in vivo* imaging of basal cell carcinomas.(BCCs) [8-10] RCM has been introduced recently in clinical dermatology fields, and may be a novel instrument. It enables us the *in vivo* non-invasive observation of the skin lesions at the level of histological resolution ( approximately 0.5 □m in the lateral dimension and 3..2 □m in the axial ones to a depth of 350 □m). It produces pictures representing horizontal planes of skin lesions.[4, 5]

Here we investigated if "early /or micro" lesions of BCC could be accurately diagnosed by combined observation of dermoscopy and RCM...

**Materials and methods:**

Five BCC lesions from four patients were investigated by dermoscopy and subsequently by *in vivo* or *ex vivo* RCM, i.e., RCM examination before and after surgical excision respectively. Dermoscopy followed the two-step method of the "consensus net meeting on dermoscopy 2000",[12,13] using commercially available DermoGenius basic (LINOS, Königsallee, Germany) and digital camera (Coolpix 3600, Nikon Corporation, Tokyo, Japan). Confocal imaging was performed using a commercially available RCM with a near-infrared (830nm Diode) laser (Vivascope 1500, Lucid Inc., Rochester, NY). Five % acetic acid was used to enhance images[14] (Fig B, F).

**Results:**

Five BCC lesions were investigated (Table).

Case 1: A brown plaque (10 x 8 mm) with "pearly border" (Fig 1 A). *Ex vivo* RCM revealed the following morphologic features unique to pigmented BCC. Firstly, it could elucidate the individual tumor-cell nests, and revealed bright, oval satellite-like structures, which represented aggregates of melanin pigments or melanocytes, locating in the nests of tumor cells (Fig 1 B, C). The dermal stromas surrounding tumor-cell nests (parenchyma) often showed oval reflecting bodies with some bright-colored structures which represented melanophages (Fig 1 B). Secondly, the spoke-wheel areas of dermoscopy correlated well with tumor-cell nests on RCM (Fig 1 D, E), which, however, revealed peripheral-dark area surrounding the tumor cell nests (Fig 1 B, E).. Thirdly the "spoke" of spoke-wheel areas of dermoscopy (Fig 1 D) was also shown by RCM (Fig 1E) and confirmed by vertical HE sections (Fig 1 G). The palisading and cleft formation on HE sections (Fig 1 G) correlated well with palisaded bright and peripheral dark areas on cross-sectional view of *ex vivo* RCM (Fig 2 A).

Case 2: A flat erythematous, slightly scaly lesion (10 mm in diameter) with irregular border (Fig 2C). *Ex vivo* RCM could visualize globular-tumor surface structures that were hardly detected by dermoscopy (Fig 2D, E).

Case 3: A multiple small, round pigmented BCC lesions on whole body from a nevoid BCC syndrome patient. Dermoscopy of an oval brown lesion (2 mm in diameter) on right cubital fossa could detect multiple blue-gray dots or globules and spoke-wheel like areas by digital magnification (Fig 3A). Dermoscopy of another pigmented lesion (2 mm in diameter) on right back revealed two spoke-wheel areas by digital magnification (Fig 3B). However, it was *in vivo* RCM that visualized easily not only spoke-wheel like lesions but also tumor cell nests. Besides, *in vivo* RCM could show tumor-cell nests (parenchyma) surrounded by dark areas (Fig 3C), and bright areas of tumor periphery with "star formation" (Fig 3D).

Case 4: A lesion with ulceration and telangiectasia from a Caucasian male (Fig 3 E).*Ex vivo* RCM could visualize the tumor parenchyma surrounded by dark areas (Fig 3 F).

**Discussion:**

Dermoscopy is a noninvasive optical strategy for imaging skin-tumors..[4] We found that RCM represents another imaging technology with greater resolution and contrast up to a depth of 350 µm, providing skin imaging in real time at a resolution almost equal to that of conventional microscopes...[4,5] RCM would help us to avoid unnecessary surgery by differentiating *in vivo* pigmented BCCs from other pigmented tumors and detecting "early/micro" BCC as small as 2 mm with images comparable to those of "common" BCC (larger than 5mm). RCM could visualize the peripheral dark areas surrounding tumor-cell nests (parenchyma) and the palisaded tumor cells in "early" / micro-" lesions. RCM could also identify the extent of horizontal infiltration of BCCs, which could not be recognized by dermoscopy (Fig 2 G, I). However, RCM could not define accurately the depth of tumor invasion, which is the limitation of this technology. The tumor depth can accurately be diagnosed histologically. Peripheral dark areas of decreased signal between tumor parenchyma and adjacent dermal stroma, which were reported by Vinh Q *et al,*[15] were found to represent clefts accumulated with mucinous substances in HE sections...[16] Lacunae, which are regarded as a fixation artifact, but can also be observed on cryostat section,[16] have been thought to correspond to "dark areas" by *in vivo* RCM (Fig 3 D, F)... Our study of *in vivo* and *ex vivo* RCM confirmed that these areas represent loose stroma accumulated with mucinous substances on HE sections. These findings were not seen by RCM in any other skin tumors, e.g., malignant melanoma, dermatofibroma, soft fibroma, trichoepithelioma, seborrheic keratosis, dermatofibrosarcoma protuberance, Merkel cell carcinoma and solar lentigo that we have examined in this study as controls (data was not shown). Thus, RCM finding of "dark areas" surrounding tumor parenchyma is a unique, diagnostic sign for "early" / micro-" lesion of BCC..

In our case #2 and #4, dermoscopy revealed ulceration and arborizing vessels, but not dots or globules. RCM, however, demonstrated clearly bright tumor parenchyma and dark peripheral areas (Fig 2 E). RCM could well demonstrate tumor margin of pigmented / non-pigmented BCC, but there is a limitation to visualize the entire tumor border, though we could identify globular tumor-surface structure in our case #3 which was less than 3 mm in size (Fig 3 C). The current RCM technology can only show the limited lesions of full-size XY-maps and any lesion larger than 3..0- 3.5 mm will not 'fit' on the screen in its entirety..

In "early / micro-" lesions of BCC, dermoscopy allowed us to visualize the multiple blue-gray dot or globules and spoke-wheal areas by magnification with digital camera (Fig 3 A, B). However, RCM could easily visualize spoke-wheel like structures which we called "star formation" (Fig 3 D). Hence, the combined observation of dermoscopy and

RCM is useful for diagnosing "early / micro" lesions of BCC that dermoscopy alone can hardly detect. RCM identifies not only the surface structure of BCC but also their inside structure, i.e., "dark areas" surrounding the tumor-cell nests. These RCM features appear to be diagnostic for BCCs, specifically for "early / micro-" lesions. Their sensitivity and specificity, however, need to be tested by additional large studies.

## References


1 Zalaudek, I., Argenziano, G., Soyer, H. P et al. Three-point checklist of dermoscopy: an open internet study. Br J Dermatol 2006; 154:431-437.

2 Rallan, D., Bush, N. L., Bamber, J. C et al. Quantitative discrimination of pigmented lesions using three-dimensional high-resolution ultrasound reflex transmission imaging. J Invest Dermatol 2007; 127:189-195.

3 Gambichler, T., Orlikov, A., Vasa, R et al. In vivo optical coherence tomography of basal cell carcinoma. J Dermatol Sci 2007; 45:167-173.

4 Ruocco, E..., Argenziano, G., Pellacani, G et al. Noninvasive imaging of skin tumors. Dermatol Surg 2004; 30:301-310.

5 Rajadhyaksha, M..., Gonzalez, S., Zavislan, J. M et al. In vivo confocal scanning laser microscopy of human skin II: advances in instrumentation and comparison with histology. J Invest Dermatol 1999; 113:293-303.

6 Busam, K. J., Charles, C., Lohmann, C. M et al. Detection of intraepidermal malignant melanoma in vivo by confocal scanning laser microscopy. Melanoma Res 2002; 12:349-355.

7 Rajadhyaksha, M., Grossman, M., Esterowitz, D et al. In vivo confocal scanning laser microscopy of human skin: melanin provides strong contrast. J Invest Dermatol 1995; 104:946-952.

8 Nori, S., Rius Diaz, F., Cuevas, J et al. Sensitivity and specificity of reflectance-mode confocal microscopy for in vivo diagnosis of basal cell carcinoma: a multicenter study. J Am Acad Dermatol 2004; 51:923-930.

9 Sauermann, K., Gambichler, T., Wilmert, M et al. Investigation of basal cell carcinoma [correction of carcionoma] by confocal laser scanning microscopy in vivo. Skin Res Technol 2002; 8:141-147.

10 Gonzalez, S., Tannous, Z.. Real-time, in vivo confocal reflectance microscopy of basal cell carcinoma. J Am Acad Dermatol 2002; 47:869-874.

11 Charles, C. A., Marghoob, A. A., Busam, K. J et al. Melanoma or pigmented basal cell carcinoma: a clinical-pathologic correlation with dermoscopy, in vivo confocal scanning laser microscopy, and routine histology. Skin Res Technol 2002; 8:282-287.

12 Rajadhyaksha, M., Menaker, G., Flotte, T et al. Confocal examination of nonmelanoma cancers in thick skin excisions to potentially guide mohs micrographic surgery without frozen histopathology. J Invest Dermatol 2001; 117:1137-1143.

13 Argenziano, G., Soyer, H. P., Chimenti, S et al. Dermoscopy of pigmented skin lesions: results of a consensus meeting via the Internet. J Am Acad Dermatol 2003; 48:679-693.

14 Menzies, S. W., Westerhoff, K., Rabinovitz, H et al. Surface microscopy of pigmented basal cell carcinoma. Arch Dermatol 2000; 136:1012-1016.

15 Chung, V... Q., Dwyer, P. J., Nehal, K. S et al. Use of ex vivo confocal scanning laser microscopy during Mohs surgery for nonmelanoma skin cancers. Dermatol Surg 2004; 30:1470-1478.

16 Kirkham N. Tumors and cysts of the epidermis. In: Lever's Histopathology of the Skin.9th edition. Elder DE, Elenitsas R, Jaworsky C, Johnson B Jr, editors. Lippincott Williams & Wilkins. 2005; 842.

**Figure legends**

Figure 1.

A.: Dermoscopic view of case 1, showing multiple blue-gray globules (blue arrows), arborizing vessels (white arrows), spoke-wheel areas (white arrow-heads) and maple-leaf like areas (red arrows). (scale bar: 1.0 mm). An insert shows a brown plaque of BCC (10× 8 mm ) with "pearly border".

B-C: Comparison of *ex vivo* RCM and histopathological view of BCC lesion shown in Fig 1-A, which consists of tumor-cell nests (parendryma) with irregular border.

B:Vertical *ex vivo* RCM view of the peripheral margin of tumer-cell nests which consists of palisading arrangement and irregular club-like tumor invasion, and oval
or satellite-like structures with bright-reflectance, representing clumps of melanin
pigments or melanocytes (scale bar: 50μm). Five % acetic acid was used to enhance images.

C:Horizontal *ex vivo* RCM view of irregular tumor parenchyma with peripheral bright-reflecting area, showing the palisading and dark areas. (scale bar: 100μm)

D: Dermoscopic view of spoke-wheel areas of irregularly shaped, tumor-cell nests shown in Fig1-A.

E: *Ex vivo* RCM view of Fig 1-D showing peripheral dark areas (arrow heads) of tumor margins. (scale bar: 500μm)

Figure 2

A: Vertical *ex vivo* RCM view for a cross-section of spoke, showing bright areas (arrow heads) surrounded by dark areas (arrow) that correlate well with HE section (scale bar: 50μm). Five % acetic acid was used to enhance images.

B: Vertical HE section of spoke revealing oval tumor parenchyma surrounded by the palisading arrangement and cleft formation×400.

C: Dermoscopy of case 2 revealing ulcer (arrows) and arborizing vessels (arrow head), but without dot/globules. (scale bar: 1.0 mm) An insert shows an atrophic BCC Lesion (scale bar: 10 mm).

D, E: Comparison of horizontal dermoscopic (D) and *ex vivo* RCM (E) views revealing bright-colored, tumor-cell nests surrounded by dark areas (arrow head). (scale bar: 500μm)

F: Horizontal *ex vivo* RCM view of irregular tumor parenchyma with peripheral bright-reflecting area, showing the palisading and dark areas(scale bar: 100μm).

Figure 3

A: Dermoscopy view of case 3 with multiple blue-gray globules (arrow heads) and spoke-wheel like area (arrow). An insert shows a 2-mm-sized, brown papule of BCC (scale bar: 200μm).

B: Dermoscopy of case 3 with digital magnification showing two spoke-wheel areas (arrows). An inset shows a 2-mm sized, brown papule of BCC (scale bar: 500μm).

C: Horizontal *in vivo* RCM of case 3, revealing spoke-wheel areas of dermoscopy (B), which correlate to tumor-cell nests with irregular borders surrounded by dark-gray areas of *in vivo* RCM. (scale bar: 500μm)

D: *In vivo* RCM view revealing star-shaped, tumor margin which is surrounded by dark-gray areas and peripheral bright portions. A spoke-wheel like structure which we called "star formation". (scale bar: 100μm)

E: Dermoscopy of case 4, revealing ulcer and arborizing vessels, but without dot/globules (scale bar: 5mm). An insert shows a 2-mm- sized, ulcerating BCC with peripheral telangiectasia.

F: *Ex vivo* RCM of case4, revealing peripheral-dark areas which surround the tumor parenchyma(scale bar: 50μm). The tumor was excised 3 mm free margin from the tumor and processed to ex vivo RCM.

| Case | Dermosocpy | CSLM |
|---|---|---|
| #1. 80 y.o. male | • Multiple blue-gray globules<br>• Arborizing vessels<br>• Spoke wheel areas<br>• Maple leaf-like areas | • Irregular tumor parenchyma wiith palisaded bright area<br>• Dark area surrounding tumors |
| #2. 75 y.o. female | • Ulcer<br>• Arborizing vessels | • Tumor invasion<br>• Dark area surrounding tumor parenchyma |
| #3. 52 y.o. female | | |
| a) | • Multiple blue-gray globules<br>• Spoke wheel-like area | Not done |
| b) | • Spoke wheel areas | • Star-shaped irregular tumor with palisaded bright area<br>• Dark area surrounding tumor parenchyma |
| #4. 49 y.o. male | • Ulcer<br>• Arborizing vessels | • Star-shaped irregular tumor with palisaded bright area<br>• Dark area surrounding tumor parenchyma |

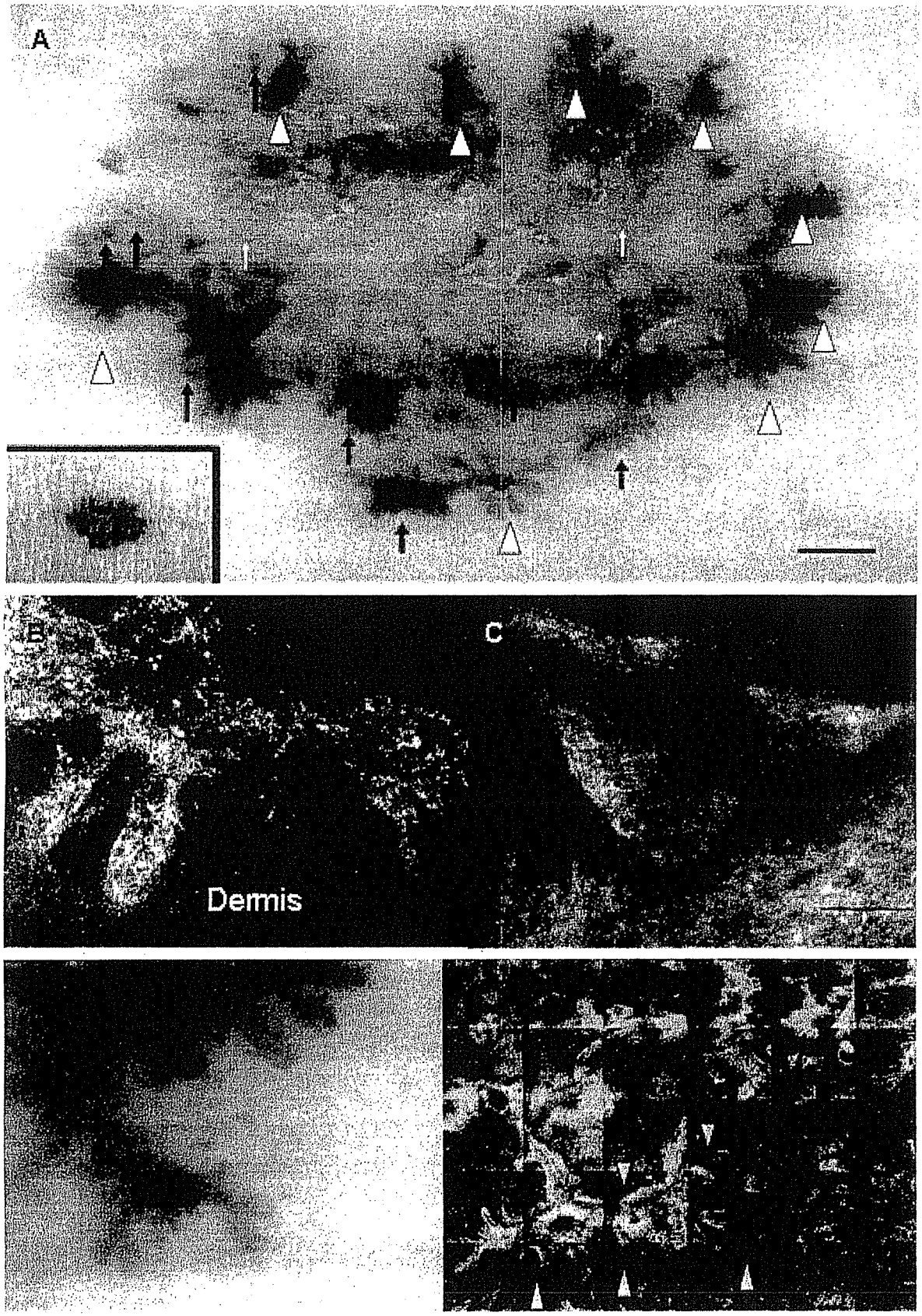
A
B
C
Dermis

A
B
C
D
E

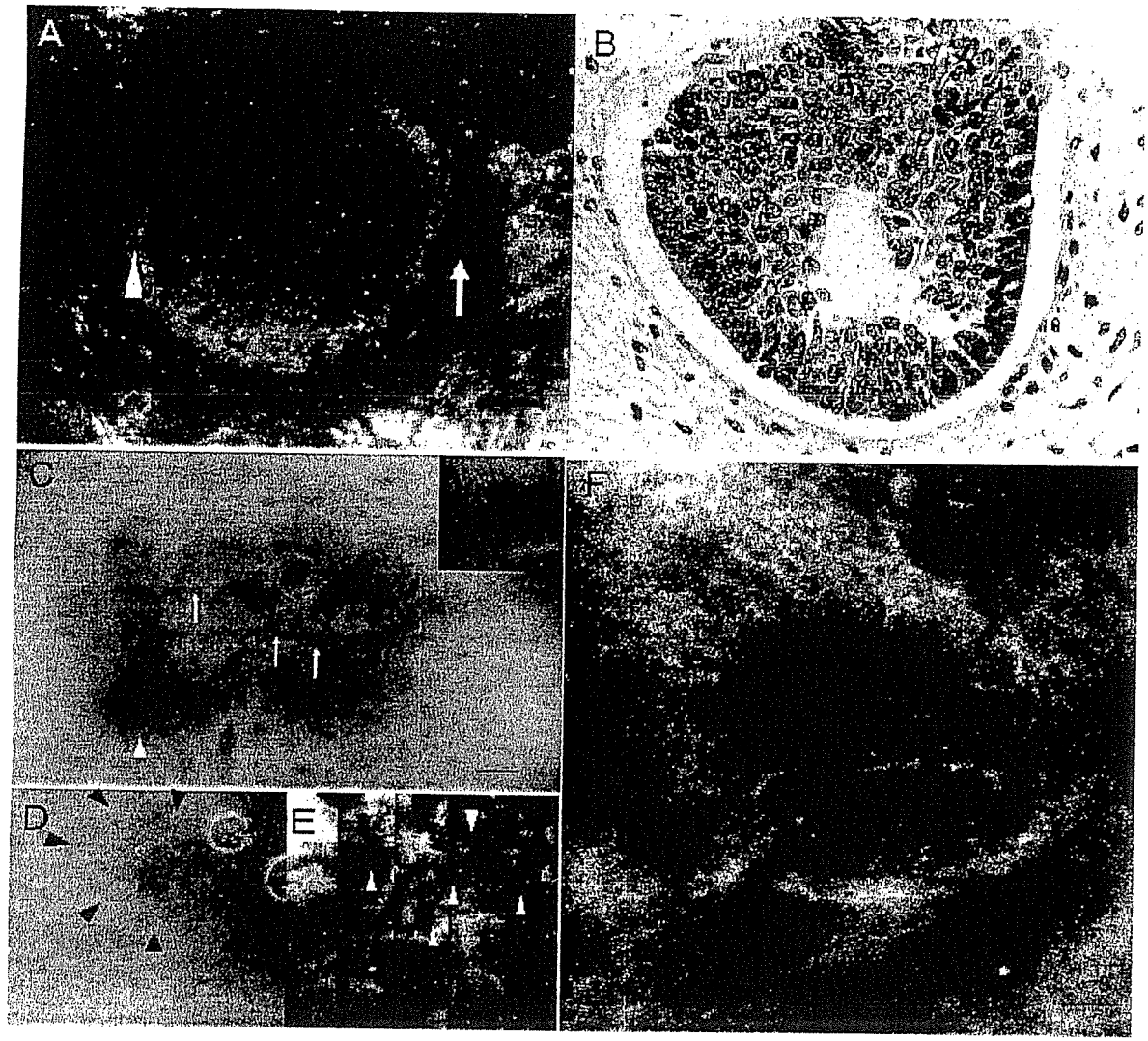
A
B
C
D
E
F